



# Effects of Prandtl Number on Three Dimensional Coherent Structures in the Wake behind a Heated Cylinder

S. Ajith Kumar <sup>1†</sup> and S. Anil Lal<sup>2</sup>

<sup>1</sup> *Department of Mechanical Engineering, Amrita Vishwa Vidyapeetham, Amritapuri, India-690525*

<sup>2</sup> *Department of Mechanical Engineering, College of Engineering Trivandrum, Thiruvananthapuram, India-695017*

†*Corresponding Author Email: ajithkmrs@gmail.com*

(Received April 1, 2020; accepted July 17, 2020)

## ABSTRACT

Flow past a heated cylinder kept at constant surface temperature is computationally simulated and analyzed in the laminar regime at moderate buoyancy. In this study, we have restricted to moderate Reynolds numbers to completely eliminate the presence of mode-A and mode-B instabilities. The three dimensional transition due to the mode E instability is captured using a cell-centered finite volume method. The present study reveals the existence of two different kinds of coherent structures - the “surface plumes” and the “mushroom structures”. The role of these mushroom structures in the heat transfer mechanism and the changes that the Prandtl number would bring into this coherent structure are discussed. The mushroom structures observed show high dependency on the changes in Prandtl number whereas the surface plumes are found almost unaffected.

**Keywords:** Thermal convection; Cross-flow; Mixed convection;  $\Lambda$ -vortices; Mushroom structures.

## NOMENCLATURE

<b>b</b>	source term vector for mixed convection flow	<b>u</b>	velocity vector
$C_L$	coefficient of lift	$U$	dimensional X component of the velocity
$C_D$	coefficient of drag	$U_0$	free stream velocity
$D$	diameter of the cylinder	$u_\theta$	non dimensional tangential velocity on the cylinder surface
Gr	Grashoff number	$V$	dimensional Y component of the velocity
$g$	acceleration due to gravity	$W$	dimensional Z component of the velocity
$n$	normal to the boundary	<b>x</b>	non-dimensional spatial coordinate vector
$Nu_\theta$	local Nusselt number	$x$	non-dimensional spatial X coordinate
$Nu_{avg}$	average Nusselt number	$y$	non-dimensional spatial Y coordinate
$p$	non-dimensional pressure	$z$	non-dimensional spatial Z coordinate
Pr	Prandtl number	$\nu$	kinematic viscosity of the fluid
$r$	$\sqrt{x^2 + y^2}$ denotes the cylinder surface	$f$	vortex shedding frequency
Re	Reynolds number	$\Theta$	non-dimensional temperature
Ri	Richardson number	$\rho_0$	free stream density
St	Strouhal number	$\beta$	thermal expansion coefficient
$t$	non-dimensional time	$\Delta T$	temperature difference
$T_0$	free stream temperature		
$T_w$	cylinder wall temperature		
$T$	dimensional temperature		

$\alpha$	thermal diffusivity	$\omega_y$	y component of the vorticity
$\theta$	the polar angle evaluated from the rear stagnation point	$\omega_z$	z component of the vorticity
$\phi$	any of the scalars u, v, w or $\Theta$	$\Delta r_i / \Delta r_{i-1}$	Stretching ratio in the radial direction
$ \omega $	magnitude of the absolute value of vorticity	$\Delta x_i / \Delta r_{i-1}$	Stretching ratio in the x direction
$\omega_x$	x component of the vorticity	$\Delta y_i / \Delta r_{i-1}$	Stretching ratio in the y direction

## 1. INTRODUCTION

Over the past few decades, a number of studies [Taneda (1956), Williamson and Roshko (1990), Roshko (1993), Williamson (1996b), Zdravkovich (1997), Sen *et al.* (2009), Rajani *et al.* (2016)] have focused on the wake structure analysis of flow past a cylinder at low Reynolds number,  $Re(= U_0 D / \nu)$ , defined as the ratio of inertial forces to the viscous forces. Here  $U_0$  is the free stream velocity,  $D$  the diameter of cylinder, and  $\nu$  the kinematic viscosity of the fluid. A plethora of issues like the aerodynamic forces, boundary layer phenomena, vortex induced vibrations, the transition to turbulence etc. have been investigated in the canonical case of flow past a circular cylinder.

Three dimensionality of the flow past cylinder has been a topic of interest for past several decades. Oblique shedding is the one which attributes to the spanwise three dimensionality of the flow. Eisenlohr and Eckelmann (1989) observed that the oblique shedding can be controlled with the help of end plates mounted on the cylinder. However, this paper does not focus on the three dimensionality of the flow due to oblique shedding and considers parallel shedding mode. The other kind of three dimensionality is due to the instabilities present in the flow. Hama (1957) established that the instabilities present in flow past bluff bodies are in the form of three dimensional spanwise waves. Later, Gerrard (1978) observed similar spanwise waviness in his experiments and he named it as "finger of dye". DNS computations with higher order spectral accuracy conducted by Karniadakis and Triantafyllou (1992) established that the flow becomes inherently three dimensional when  $Re > 200$ . It was Williamson (1996a) who interpreted these instabilities as mode-A and mode-B, depending on the range of  $Re$  at which it occurs and by its own unique characteristics. Three dimensional instabilities comes into picture above  $Re = 180$ . Williamson (1996c), in his experiments showed that two types of instabilities exist which turn the two dimensional flow into a three dimensional flow. Mode-A corresponds to the  $Re$  range of 180-190 and mode-B exists in the range of 230-260, which is clearly shown in Strouhal number- $Re$  relation curve in Williamson (1988). The Strouhal number,  $St(= fD/U_0)$  is the non-dimensional form of shedding frequency,  $f$ . According to Williamson (1996a), the elliptical instability is responsible for the "finger of dye" (spanwise waviness) above  $Re = 180$ . Though both modes of instabilities triggers

three dimensionality in the flow, they have distinguishable inherent physical behaviours. Mode-A instability has a spanwise wavelength of 3-4 cylinder diameters and mode-B instability has a spanwise wavelength of 1 cylinder diameter Williamson (1996a). The study of instability mechanisms and the formation of 3D vortical structures can contribute to the understanding of laminar-turbulent transition and lead ways to control the flow.

Heating the cylinder surface imparts characteristic changes to the flow behaviour and this situation has immense industrial applications (cooling towers, heat exchangers, chimney stacks etc.) and is a favourite topic for many academicians. In most of the experimental studies on flow over heated cylinders, buoyancy effects are considered almost zero, though it exists in reality. The zero buoyancy assumption is valid only at conditions where the temperature difference between the cylinder and the cold fluid flowing over it is very small. The present study focuses on mixed convection flows where the buoyancy effects are also considered. Richardson number ( $Ri$ ) is the non-dimensional number representing the magnitude of buoyancy force over the inertia force, whose expressions are given in section 2. Mahir (2017) has performed computational investigation on forced convection flow over an isothermal square cylinder and found that the mode-A and mode-B instabilities influence the three dimensional heat transfer. Tanweer *et al.* (2019), Ajith Kumar *et al.* (2016a) and Sarkar *et al.* (2011) have investigated the effects of Prandtl number on convective heat transfer from a heated horizontal cylinder and reported that the heat transfer is significantly affected by the changes in  $Pr$ . According to Wang *et al.* (2000), the flow can be assumed free from buoyancy forces only if the  $Ri < 0.02$ . The buoyancy effects are very close to zero in the other experiments reported by Lecordier *et al.* (1991) and Vít *et al.* (2007). Kieft *et al.* (2002) and Ajith Kumar *et al.* (2016b) proposed that when  $Ri > 0.02$ , buoyancy will bring asymmetry in the flow in an otherwise perfectly symmetrical flow pattern. They claim that flow past a heated cylinder will generate alternate rows of vortices with different vortex strengths due to the production of baroclinic vorticity. In fact, buoyancy has an important role to play in three dimensional transition and in triggering turbulence. Ren *et al.* (2004) reported that three dimensional effects can be seen for flow over heated cylinder when  $Ri > 0.35$  and  $85 < Re < 117$  and named the instability responsible for this as

mode-E. The occurrence of mode-E transition in flow past a heated cylinder is also reported in literature, [Kieft et al.\(2002\)](#), [Ren et al. \(2006\)](#), [Rolfo et al. \(2018\)](#) but not well documented. Table 1 shows the different modes of instabilities which is attributed to the three dimensional nature of the wake behind the cylinder and the ranges of  $Re$ ,  $Ri$  and  $Pr$  at which they are seen. It can be seen from the table 1 that three dimensional transition happens easily in the case of flow past heated cylinder, as compared to the unheated scenario, which is the scope of the work. In the present study, we performed extensive computations to simulate the three dimensional wake patterns due to the mode-E instability behind the heated cylinder at moderate Reynolds number.

**Table 1 Different modes of instabilities present in flow over circular cylinder with and without heating, reported by [Williamson \(1996c\)](#) and [Ren et al. \(2004\)](#). Here  $D$  represents the diameter of the cylinder**

Mode	$Re$	$Ri$	$Pr$	Wave length
Mode-A	180-190	0	7	$3-4D$
Mode-B	210-230	0	7	$1D$
Mode-E	85-117	1	7	$2D$

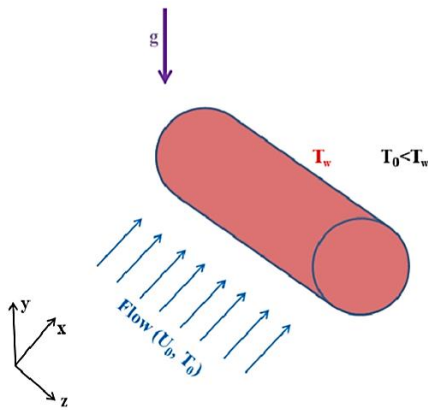


**Fig. 1. Schematic representation of the problem analyzed in this paper.**

A schematic representation of the problem being analysed in this paper is shown in Fig. 1. The cold flow at free stream conditions  $(U_0, T_0)$  takes place over a cylinder kept at uniform elevated temperature  $T_w$ . The acceleration due to gravity,  $g$  acts vertically downwards along the negative  $y$  direction. The ranges of parameters considered in this numerical work are:  $75 \leq Re \leq 150$ ,  $0.5 \leq Ri \leq 2$  &  $0.25 \leq Pr \leq 10$ . In this regime of Reynolds numbers, mode-A and mode-B instabilities are not present and the three dimensionality arising is only due to buoyancy (mode-E). This paper discusses the occurrence of the three dimensionality due to mode-E instability, the characteristics of coherent structures formed behind the heated cylinder and the effects of Prandtl number on these coherent structures.

## 2. NUMERICAL METHOD

The buoyancy driven flow from a heated cylindrical surface, whose temperature is held constant, interacts with the laminar mean flow to yield mixed convection conditions. The governing partial differential equations in the Cartesian coordinate system used to simulate the problem are incompressible continuity, Navier-Stokes and energy equations. The dimensionless forms of equations for momentum, continuity and energy under the Boussinesq approximation for the problem being investigated are given in Eqs 2 to 3.

$$\nabla \cdot \mathbf{u} = 0, \tag{1}$$

$$\frac{\partial \mathbf{u}}{\partial t} + \mathbf{u} \cdot \nabla \mathbf{u} = -\nabla p + \frac{1}{Re} \nabla^2 \mathbf{u} + \mathbf{b}, \tag{2}$$

$$\frac{\partial \Theta}{\partial t} + \mathbf{u} \cdot \nabla \Theta = \frac{1}{RePr} \nabla^2 \Theta. \tag{3}$$

where  $\mathbf{b} = [0 \ Ri \ \Theta \ 0]^T$  is the source term for mixed convection flow, derived using Boussinesq approximation. The cylinder diameter,  $D$  and the free stream velocity  $U_0$  are taken as the reference scales to non-dimensionalize the spatial coordinate vector and the velocity vector as follows.  $\mathbf{x} = [x \ y \ z]^T = [X/D \ Y/D \ Z/D]^T$  and  $\mathbf{u} = [u \ v \ w]^T = [U/U_0 \ V/U_0 \ W/U_0]^T$ .

The non-dimensional temperature  $\Theta$  is defined as  $\Theta = (T - T_0)/(T_w - T_0)$ , where  $T$  is the dimensional temperature,  $T_0$  is the constant free stream temperature and  $T_w$ , the constant cylinder wall temperature. The pressure,  $p$  is non-dimensionalized with the dynamic pressure,  $\rho_0 U_0^2$ . The free stream density and temperature are indicated by  $\rho_0$  and  $T_0$  respectively. The two non-dimensional numbers appearing in the Eqs (2)-(3) are the Richardson number  $Ri$  and the Prandtl number  $Pr$  and are defined as below.

$$Ri = \frac{Gr}{Re^2} = \frac{\beta g \Delta T D}{U_0^2} \tag{4}$$

$$Pr = \frac{\nu}{\alpha} \tag{5}$$

where  $Gr = \frac{\beta g \Delta T D^3}{\nu^2}$  is the Grashoff number,

$\beta, g, \Delta T, \nu$  and  $\alpha$  are the thermal expansion coefficient, acceleration due to gravity, temperature difference, kinematic viscosity and thermal diffusivity respectively. In this paper,  $Ri = 0$  is interpreted as zero buoyancy.

A Collocated finite volume method is employed to solve the governing Eqs (2)-(3) numerically using the Projection method (details of the projection method is illustrated in [Anil Lal et al. \(2012\)](#)). A

fully explicit central difference scheme is developed with first order Euler time marching scheme to capture the flow dynamics. Conjugate gradient method is used to solve the pressure Poisson equations accurately (Saad 2003).

The fully explicit method for time integration is subjected to the Courant-Friedrichs-Lewy (CFL) stability criterion. In addition, the mass flow error is computed conventionally and is used for checking the divergence of velocity vector at every time step. Finally, the  $L_2$  norm of the errors of velocities, mass and temperature are monitored and the convergence criterion is set as  $10^{-6}$ . This criterion for convergence is strictly valid only for steady flows, and therefore the temporal evolution of other integral quantities such as the lift & drag coefficients and the average Nusselt number are checked for flows that converge to an unsteady, oscillatory state. The aerodynamic force coefficients  $C_L$  and  $C_D$  are computed as:

$$C_L = \int_0^{2\pi} \left( -p \sin\theta + \frac{1}{Re} \frac{\partial u_\theta}{\partial r} \cos\theta \right) d\theta, \quad (6)$$

$$C_D = \int_0^{2\pi} \left( -p \cos\theta - \frac{1}{Re} \frac{\partial u_\theta}{\partial r} \sin\theta \right) d\theta, \quad (7)$$

where  $r = \sqrt{x^2 + y^2}$  denotes the cylinder surface and the subscript  $\theta$  being the polar angle evaluated from the rear stagnation point of the cylinder in the anticlockwise direction as shown in Fig. 2 (inset). The tangential velocity on the cylinder surface is represented by the symbol  $u_\theta$ .

The heat transfer occurring at the cylinder surface is best described using the relative magnitudes of convection and conduction, quantified by the Nusselt number. The Nusselt number  $Nu_\theta$  is defined as (Verzicco and Camussi 1997):

$$Nu_\theta = - \frac{\partial \Theta}{\partial r} \Big|_{\text{on the cylinder surface}} \quad (8)$$

The average Nusselt number  $Nu_{avg}$  is obtained by integrating  $Nu_\theta$  around the entire cylinder surface:

$$Nu_{avg} = \frac{1}{2\pi} \int_0^{2\pi} Nu_\theta d\theta. \quad (9)$$

### 3. VALIDATION

The present three dimensional numerical scheme is validated for flow around a circular cylinder and the results obtained are discussed in this section. The computations are done for  $Re = 100$ ,  $Ri = 0$  and  $Pr = 0.7$  case for the validation, as the data for the three dimensional cases with non-zero Richardson number is not available. The strouhal number,  $St$  is evaluated for  $Re = 100$ ,  $Ri = 0$  and  $Pr = 0.7$  and is compared with literature and is consolidated in table 2. A good agreement of the computed values are seen with those reported in the literature with a maximum deviation of less than 4%.

### 4. DOMAIN AND GRID INDEPENDENCE TEST

A rectangular domain with dimensions as shown in Fig. 2 is selected to perform the numerical simulation. The dimensions of the domain are fixed after conducting a domain independence test. For this, three different domains are selected as shown in table 3 and computations are performed for  $Re = 100$ ,  $Ri = 1$  and  $Pr = 0.7$ . The spanwise length is taken as 4D for all the three configurations in the table.

**Table 2 Comparison of  $St$  computed in the present study with the previous works for  $Re = 100$ ,  $Ri = 0$  and  $Pr = 0.7$**

Literature	$St$
Williamson (1996c)	0.164
Le et al. (2006)	0.160
Russell and Jane Wang (2003)	0.169
Calhoun (2002)	0.175
Mittal and Raghuvanshi (2001)	0.168
Present	0.168

**Table 3 Domain independence test: Comparison of  $St$ ,  $C_L$  and  $Nu_{avg}$  for different domain sizes at  $Re = 100$ ,  $Ri = 1.0$  and  $Pr = 0.7$ . The spanwise dimension is taken as 4D in all the cases. Here ‘M’ indicates ‘in millions’**

length	height	cells	$St$	$C_L$	$Nu_{avg}$
29D	9D	3.92M	0.194	-1.308	5.18
31D	11D	4.61M	0.192	-1.283	5.320
33D	13D	5.8M	0.191	-1.271	5.385
35D	15D	7.1M	0.191	-1.271	5.387

The non-dimensional velocity components at the inlet of the computational domain are  $u = 1.0, v = 0.0$  and  $w = 0.0$  and the temperature boundary conditions  $\Theta = 0$ . No-slip boundary condition is supplied on the hot cylinder surface with temperature condition  $\Theta = 1$ . The outlet and the four surrounding boundaries are subjected to stress-free conditions, i.e.  $\nabla \phi \cdot n = 0$ , where  $\phi$  is one of the scalars  $u, v, w$  and  $\Theta$ . It is seen that for a domain larger than  $33D \times 13D$ , the computed quantities such as  $St$ ,  $C_L$  and  $Nu_{avg}$  etc. are consistent, which is an indication that the results are not influenced by changing the size of the domain above  $33D \times 13D$ . We also compared (i) the instantaneous values of u-velocity from  $t = 130$  to 140, at  $(x, y, z) = (2D, 0, 2D)$ , downstream of the cylinder and (ii) the time averaged u-velocity profile along the  $y$  direction at  $(x, z) = (2D, 2D)$ , in the wake of the cylinder to further confirm the domain independence. The variations are given in Fig. 3. The

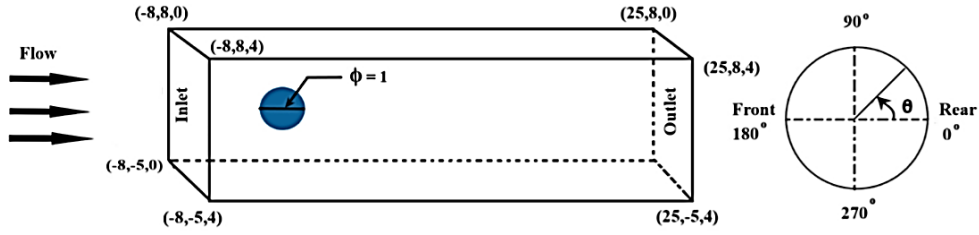


**Fig. 2.** Computational domain along with the coordinates used for the numerical validation of 3D cross-flow over a heated cylinder. The figure in the inset indicates the polar diagram defining  $\theta$ .  $\theta = 0^\circ$  at the rear stagnation point and  $180^\circ$  at the front stagnation point. The polar angle,  $\theta$  increases from the rear stagnation point when moved in the anticlockwise direction.

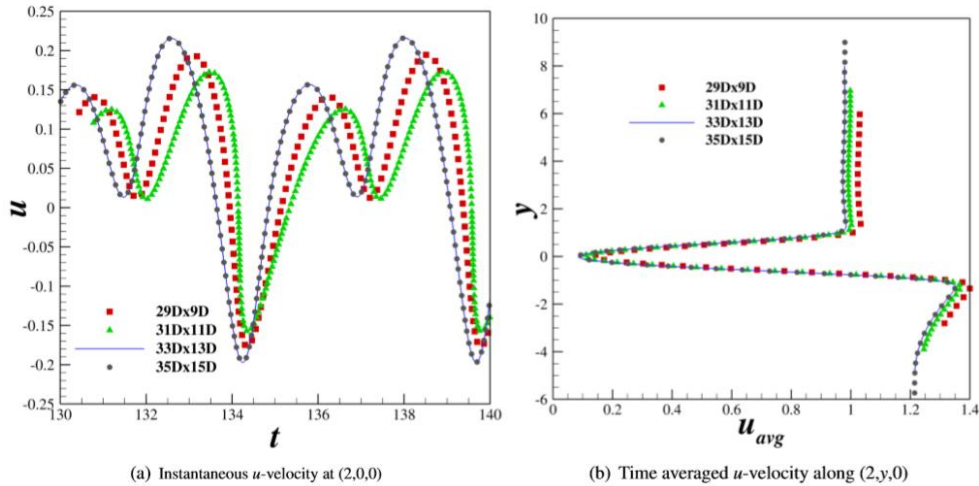


**Fig. 3.** Instantaneous and time averaged  $u$ -velocity profiles plotted for  $Re = 100$ ,  $Ri = 1$  and  $Pr = 0.7$ . Four different computational domains have been compared in these plots.

comparisons show that the 33Dx13D sized domain selected for the study is appropriate. Hence this dimension is taken for further computations in this paper for the three dimensional analysis.

A grid independence test is conducted on the selected domain to obtain the optimum number of grid. The details of the grid independence test is consolidated in table 4 which shows almost no difference in the computed values such as  $St$ ,  $C_L$  and  $Nu_{avg}$  etc. for a grid size larger than 5.8 million cells. Hence the optimum grid structure that could be used for the computations is selected as the one consisting of 5.8 million hexahedral cells and is used for all the 3D computations in the rest of this paper. The convergence is achieved as explained in the previous section.

**Table 4** Grid independence test: Comparison of  $St$ ,  $C_L$  and  $Nu_{avg}$  for different domain sizes at  $Re = 100$ ,  $Ri = 1.0$  and  $Pr = 0.7$ . The spanwise dimension is taken as 4D in all the cases

cells	$St$	$C_L$	$Nu_{avg}$
3.5 Million	0.199	-1.307	5.223
4.7 Million	0.194	-1.285	5.311
5.8 Million	0.191	-1.271	5.385
6.9 Million	0.191	-1.270	5.386

Although the vortex shedding could be captured, it is also desirable to work on a finer grid to filter out the more deeper and smaller scales such as the coherent structures in flow field. An O-type grid structure is generated around the cylinder to capture mode-E transition of the wake accurately. The size of the first layer of grid above the cylinder wall and stretching ratio ( $\Delta r_i / \Delta r_{i-1}$ ) are taken as 0.00115D and 0.95 respectively. The stretching ratio ( $\Delta x_i / \Delta x_{i-1}$ ) used outside the O-mesh are 0.9 in the upstream and 1.05 in the downstream x-direction. Along the y-direction, stretching ratio ( $\Delta y_i / \Delta y_{i-1}$ ) used are 1.05 and 0.95 at the top and bottom respectively. A uniform mesh distribution is provided along the Z-direction.

## 5. RESULTS AND DISCUSSION

In the present numerical study, it is observed that the surface heating would result in an early three dimensional transition for flow over circular cylinder, concurring the findings of *Ren et al. (2006)*. The three dimensional transition is characterized mainly by the 3D coherent structures. The study focuses on the evolution, characteristics and effects of Prandtl number on the surface plumes and the three dimensional mushroom structures formed in the wake, behind the cylinder. The ranges of parameters considered are:  $75 \leq Re \leq 150$ ,  $0.5 \leq Ri \leq 2$  &  $0.25 \leq Pr \leq 10$ . However, most of the results are

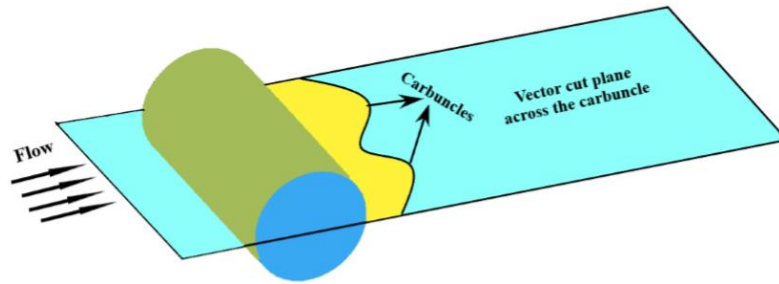


**Fig. 4. Schematic representation of the vector cut plane passing through the carbuncle. The top view of this configuration is taken to visualize the counter rotating vortices in the rest of the paper.**

presented for representative  $Re = 117$ ,  $Pr = 0.7$ , 7 and is consistent with other values of  $Re$  and  $Pr$  as well.

### 5.1 Effects of Prandtl Number on the Surface Plumes

In this section, the surface plumes (thermal plumes), which typically occur due to boundary layer instability (Sparrow *et al.* 1990) in thermal convection flows are discussed. The surface plumes are generated from the surface of hot cylinder. These plumes originate at regular intervals along the span of the hot cylinder surface. The plume locations are identified by a spike or carbuncle-like feature in the temperature contours near the cylinder surface (Ajith Kumar *et al.* 2016a). The plumes usually evolve in the direction of buoyancy, however, in the present cross-flow mixed convection condition, it evolves in a direction resulting from the mean flow (in the  $x$ -direction) and the buoyancy force due to heating (in the  $y$ -direction).

Further numerical investigations are carried out to understand the characteristics of the surface plumes. It is recalled that the surface plumes originates from the carbuncles of the iso-surface of temperature. The velocity vectors are plotted on a horizontal plane which contains the carbuncles of the iso-surface of temperature. The cut plane containing the carbuncles are represented schematically in Fig. 4. It should be noted that the vector cut plane selected can be different for another combination of  $Re$ ,  $Ri$  and  $Pr$  to contain the carbuncle. Figure 5 shows the iso-surface of temperature ( $\Theta = 0.5$ ) and the velocity vectors at a horizontal plane containing the carbuncles (top view of Fig. 4), plotted for  $Re = 117$ ,  $Ri = 1$  and  $Pr = 0.7$ . In this figure, the carbuncles are seen within the wake region with a pair of counter-rotating vortices on either side of it (the counter-rotating pair of vortices are identified with the help of the velocity vectors). The origin of the surface plumes are identified by the carbuncles in the iso-surface of temperature as shown in Fig. 5. The surface plumes are essentially “buoyant jets” and the counter rotating vortex pairs are the outcome of these “buoyant jets”. Several pairs of counter rotating vortices are seen on either side of the carbuncle (see Fig. 5), confirming the origin of the surface plumes from the cylinder surface.

It is recalled that the wave number is a parameter, which characterizes the nature of the instability being present, as indicated in table 1. The wave number is

defined as the number of waves present per unit spanwise length. There are four pairs of counter rotating vortices seen in Fig. 5, which lead us to infer that the wave number corresponding to this flow is nearly 2, as the spanwise length of the domain is  $8D$ . This confirms that the mode-E instability has wave number 2 for  $Re = 117$ ,  $Ri = 1$  and  $Pr = 0.7$ , as reported by the previous re-searchers.

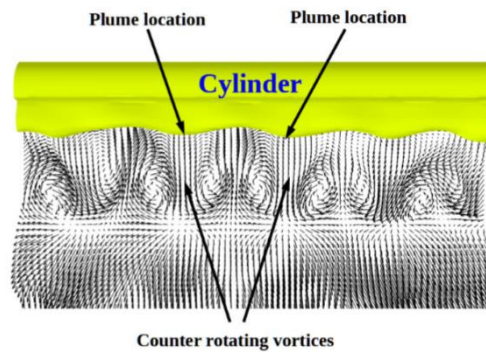


**Fig. 5. Iso-surface of temperature for  $\Theta = 0.5$  and the vector plot on a horizontal plane containing the carbuncles is plotted for  $Re = 117$ ,  $Ri = 1$  and  $Pr = 0.7$ . Each pair of counter rotating vortices is seen within the wake region about either side of the carbuncle which confirms the generation of buoyant plumes from the carbuncles.**

Gebhart *et al.* (1970), in their experimental studies showed that the number of surface plumes generated from a hot surface has strong dependency on the buoyancy force. Stronger the buoyancy force, more will be the thermal plumes generated from the heat source. Nevertheless in flow over a heated circular cylinder, an early three dimensional transition happens due to mode-E instability, which is characterized by the surface plumes. Figures 6 shows the iso-surface of the temperature for  $\Theta = 0.5$  and the vector plot on a horizontal plane containing the carbuncles plotted for different combinations of  $Re$ ,  $Ri$  and  $Pr$ . In Fig. 6, the two columns indicate  $Re = 117$ ,  $Pr = 0.7$  and  $Re = 150$ ,  $Pr = 7$  cases plotted at different  $Ri$ . From these figures, it can be concluded that the number of plumes generated from the cylinder surface increases with increase in  $Ri$ , concurring the findings of Gebhart *et al.* (1970). However, there is no appreciable changes happened

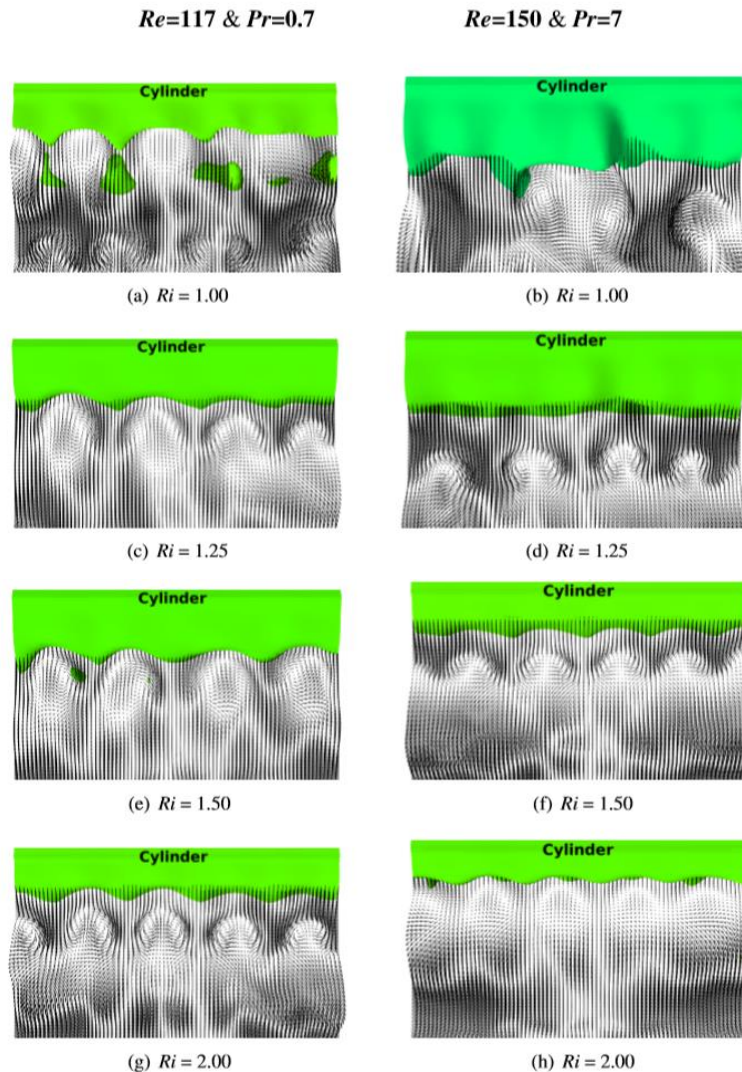


**Fig. 6.** Iso-surface of temperature for  $\Theta = 0.5$  and the vector plot on a horizontal plane containing the carbuncles is plotted for  $Re = 117$ ,  $Pr = 0.7$  and for various  $Ri$ . The number of surface plumes emanating from the cylinder surface is found to be increasing with increase in  $Ri$ .

across the columns for a different combination of  $Re$  and  $Pr$ . Hence it can be concluded that there is only marginal dependency on the  $Pr$  and  $Re$  for the number of surface plumes generated. The plume structure is also found to not change much with the changes in  $Pr$ .

Figure 7 shows the iso-surface of the temperature for  $\Theta = 0.5$  and the vorticity plotted on the same plane where the vectors are plotted in Fig. 6. These plots also confirm that the number of vortices in the plane containing the carbuncle has high dependency on the value of  $Ri$  and is influenced marginally by changes in  $Pr$ . The surface plumes are observed for all the ranges of parameters for  $Re$ ,  $Ri$  and  $Pr$  considered here. So, it can be concluded from the present numerical analysis that the occurrence of mode-E instability has even broader existence of range of parameters ( $75 \leq Re \leq 150$ ,  $0.5 \leq Ri \leq 2$  &  $0.25 \leq Pr \leq 10$ ) than that reported by [Ren et al. \(2004\)](#) ( $85 \leq Re \leq 117$ ,  $Ri = 1$ ,  $Pr = 7$ ).

## 5.2 Effects of Prandtl Number on the Mushroom Structures

When flow takes place over a cylinder above a threshold value of  $Re$  ( $\approx 47$ ), the onset of vortex shedding happens and alternate rows of vortices having opposite spinning nature start shedding behind the cylinder. When the cylinder is heated above a critical value of  $Ri$ , unstable density stratification develops at the top half region of the domain and the vortices shed from the top appeared more distorted due to the action of buoyancy. We have observed typical  $\Lambda$ -shaped structures (see Fig. 8) connecting two upper row of vortices in the wake region behind the cylinder and is termed as  $\Lambda$ -vortices in the rest of the paper. The iso-surface of vorticity is plotted in Fig. 8 for a  $|\omega| = 0.7$ . Here  $|\omega|$  is the magnitude of the absolute value of the vorticity evaluated as  $(\omega_x^2 + \omega_y^2 + \omega_z^2)^{1/2}$  and  $\omega_x$ ,  $\omega_y$  and  $\omega_z$  are respectively the  $x$ ,  $y$  and  $z$  components of the

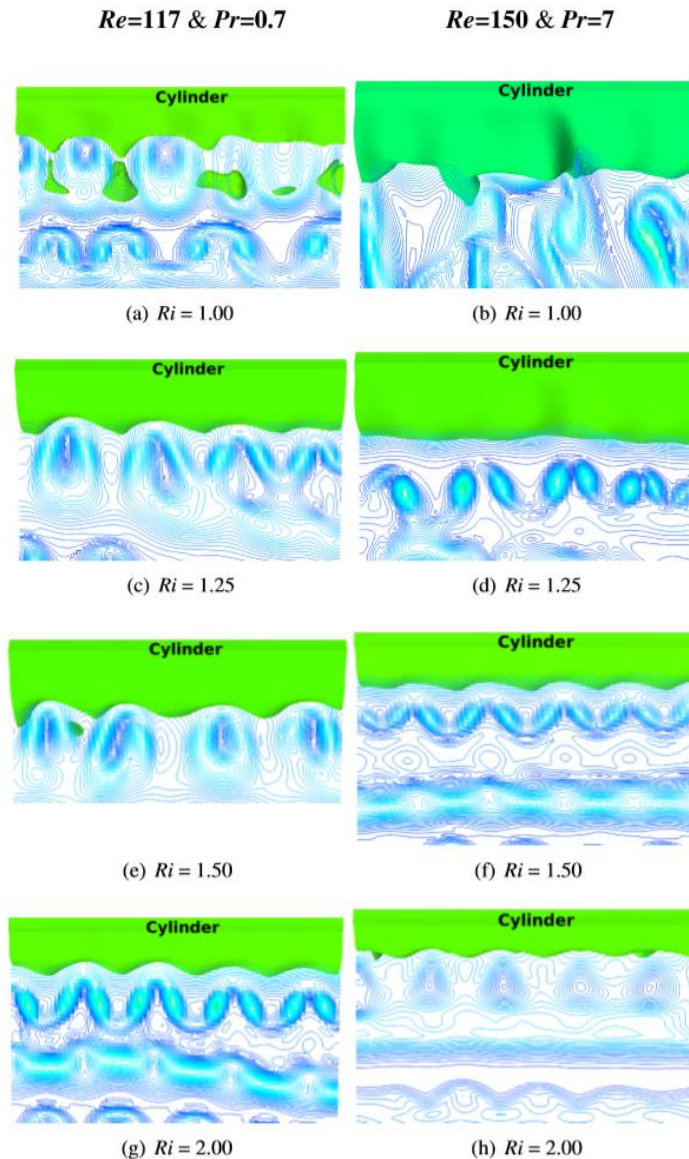


**Fig. 7. Iso-surface of temperature for  $\Theta = 0.5$  and the contours of vorticity plotted on a horizontal plane containing the carbuncles is plotted for  $Re = 117$ ,  $Pr = 0.7$  and for various  $Ri$ .**

vorticity. In this figure, the “mushroom structures” are seen escaping from each row of upper vortices. Several mushroom structures could be observed evolving from single upper vortex row. These ring like mushroom structures show good agreement with those structures observed by [Maas et al. \(2003\)](#) in their experiments.

It is seen that the mushroom structures obtained have certain distinct characteristics as seen in Figs. 11 and 12 (this is explained later). It has a cap, where the hot fluid accumulates and rises up in the direction of buoyancy and a stem, through which the continuous fluid supply is given to the cap. The stem is a neck-like region which connects the cap with the upper row of vortices. The effects of  $Pr$  on these structures are discussed later in this paper in detail.

In the numerical study, it is observed that the mushroom structures are always generated from the upper

row of vortices. No such coherent structures are found generated from the lower vortices. In Fig. 9, iso-surface of vorticity (for  $|\omega| = 0.7$ ) is plotted along with isotherms on a vertical plane, taken at a spanwise location of  $5D$  for  $Re = 117$ ,  $Ri = 1$  and  $Pr = 7$ . Similarly, in Fig. 10, iso-surface of vorticity (for  $|\omega| = 0.7$ ) is plotted along with contours of transverse velocity taken at the same spanwise location of  $5D$  for the same parameters of  $Re$ ,  $Ri$  and  $Pr$ . The iso-surface of vorticity represents the  $\Lambda$ -vortex and the bulges in the isotherms indicate the location from where the mushroom structures originates. It is clear from Fig. 9 that the origin of such structures are always between the legs of the  $\Lambda$ -vortices irrespective of  $Ri$  and  $Pr$ . Figure 10 gives confirmation to the above statement about the origin of the structures where the maximum vertical velocity is seen between the legs of the  $\Lambda$ -vortices. The fluid mass between the legs of the  $\Lambda$ -vortex lifts

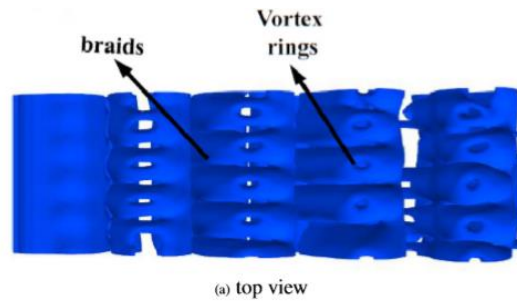


Fig. 8. Iso-surface of vorticity for  $|\omega| = 0.7$  is plotted for  $Re = 117$ ,  $Ri = 1$  and  $Pr = 0.7$ .

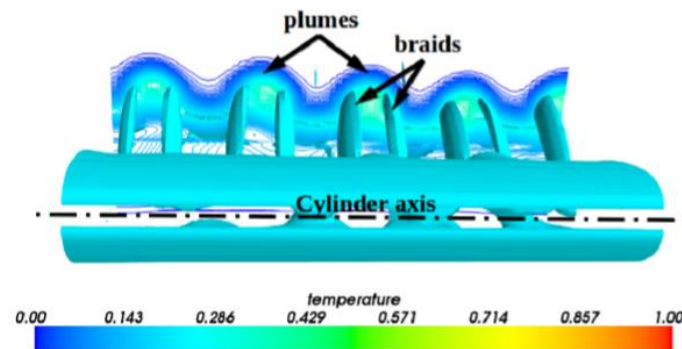


Fig. 9. Iso-surface of vorticity and temperature contour at streamwise location  $5D$ , plotted for  $Re = 117$ ,  $Ri = 1$  and  $Pr = 7$ .

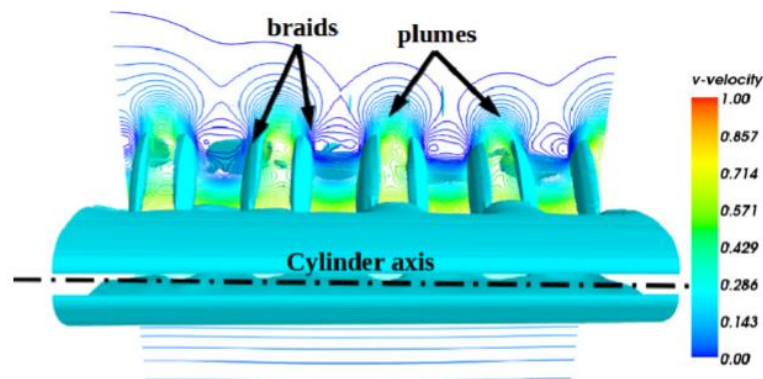


Fig. 10. Iso-surface of vorticity and contours of transverse component of velocity taken at streamwise location  $5D$ , plotted for  $Re = 117$ ,  $Ri = 1$  and  $Pr = 7$ .

up and is attributed to the origin of mushroom structures at that location.

Figures 11 and 12 show the vorticity contours and the isotherms respectively plotted at a spanwise location of  $3.7D$  for  $Re = 117$ ,  $Ri = 1$  and  $Pr = 1$ . The different parts of the structures such as cap, stem,

upper and lower rows of vortices etc. are identified and indicated in those figures. On heating the cylinder surface, unstable density stratification results in the upper half region of the domain and stable density stratification at the lower half region. Hence the upper rows of vortices which are located at the upper half region of the computational domain

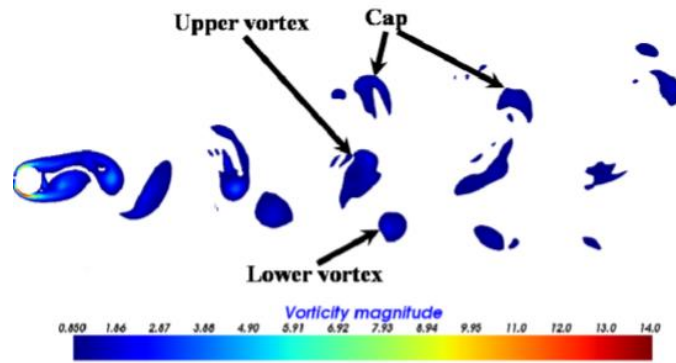


Fig. 11. Vorticity contours are plotted at a spanwise location 3.7D for  $Re = 117$ ,  $Ri = 1$  and  $Pr = 1$ . The upper vortices are more distorted and are smaller in size compared to the lower ones.

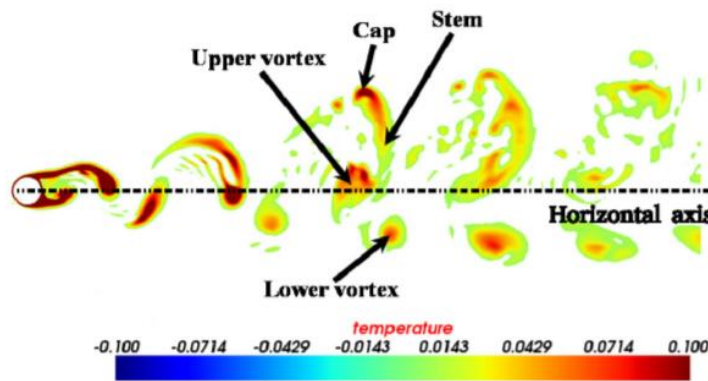


Fig. 12. Isotherms are plotted at a spanwise location 3.7D for  $Re = 117$ ,  $Ri = 1$  and  $Pr = 1$ . The dotted line indicates the horizontal axis drawn in the streamwise direction through the center of the cylinder. It is seen that the upper row of vortices shifts more away from the axis line compared to the lower row of vortex.

experiences more deformations compared with the lower rows of vortices. It can be seen more clearly in Fig. 12 that the stem of the mushroom structures always starts from the core of the upper vortex and extends to the cap. There is a supply of lighter and hot fluid from the upper vortex core to the cap of this structure through the stem, giving rise to the mushroom structures, which grows in the direction of buoyancy. The smaller size of the upper vortices is attributed to the reduced mass of fluid which is fed to the growing mushroom structures. Hence the upper rows of vortices appears both distorted and smaller in size compared to the lower vortices as seen in Fig. 11.

The shed vortices from the hot cylinder form unsymmetrical pattern in an otherwise symmetrical rows of vortices, as seen in Fig. 12. The mushroom structures emanating from each row of upper vortices acts as “buoyant jets”, results in upper vortices moving towards the horizontal center line as shown in Fig. 12. No such shifting occurs for lower vortices towards the horizontal center line since there are no mushroom structures originating from them.

To understand the effects of  $Pr$  on the mushroom structures, the iso-surface of vorticity (for  $|\omega| = 0.2$ , viewed from the top) is plotted in Fig. 13 for  $Pr = 0.25, 0.7$  and  $7$  at  $Re = 117$  and  $Ri = 1$ . The number

of mushroom structures are found to be increasing as the  $Pr$  is increased, for the same value of  $Re$  and  $Ri$ . Also they appear smaller in size at  $Pr = 7$ , compared to  $Pr = 0.25$ . At smaller  $Pr$ , the thermal diffusion is larger compared to the momentum diffusion which is attributed to the bulk size of the mushroom structures. Also the large structures are observed to be merging each other at the lower  $Pr$ .

From Figs. 11 and 12, it is understood that the vortex cores are the sources of heat as well, which indicates that the heat from the hot cylinder is mainly convected out through the shed vortices from the cylinder surface. For a fixed  $Re$  and  $Ri$ , if the  $Pr$  is increased, the thermal boundary layer thickness around each of the vortex rows get reduced which will eventually lead to an increase in heat transfer (Ajith Kumar *et al.* 2016a). This is accomplished by increasing the number of mushroom structures formed from the upper vortex and is attributed to the increase in the number of mushroom structures.

## 6. CONCLUSIONS

The three dimensional numerical study revealed about the nature of coherent structures (surface plumes and the mushroom structures) formed behind the cylinder. It is observed that the surface plumes

which originate from the hot cylinder surface are almost independent of the changes in  $Pr$  and are strongly influenced by the  $Ri$ . We found that the mushroom structures emanating from the shed vortices are responsible for a sudden (or sharp) enhancement in heat transfer from the shed vortices, and these do have a strong dependency on the  $Pr$ . These structures always form between the braids of the  $\Lambda$ -vortices. The core of the shed vortices are found to be sources of heat as well. The number of mushroom structures generated from the shed vortices increases with increase of  $Pr$ .

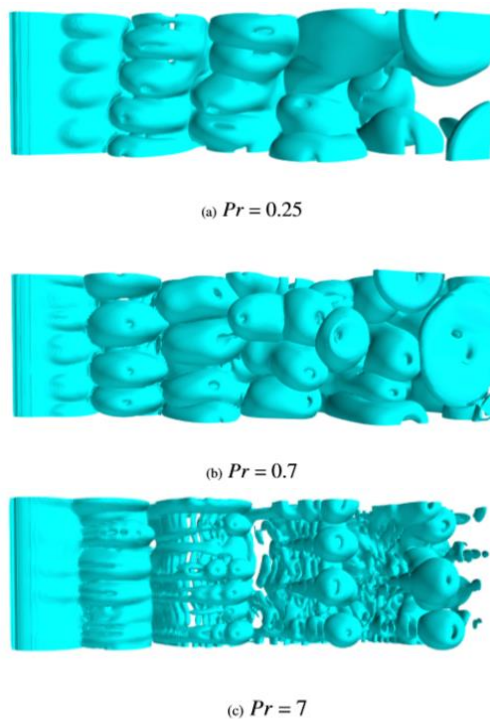


**Fig. 13.** Iso-surface of vorticity for  $|\omega| = 0.2$  is plotted for  $Re = 117$ ,  $Ri = 1$  and various values of  $Pr$ .

## REFERENCES

- Ajith, K., S., M. Mani, A. Sameen and S. Anil Lal (2016a). Effects of prandtl number on the laminar cross flow past a heated cylinder. *Physics of Fluids* 28, 113603.
- Ajith, K., S., S. Anil Lal and A. Sameen (2016b). Flow past a moderately heated horizontal cylinder at low reynolds number. *Proceedings of IMechE, Part G: Journal Aerospace Engineering* 230(7), 1224–1239.
- Anil Lal, S., R. V. Reji and K. S. Santhosh (2012). Evaluation of diffusive flux across faces of arbitrary shaped finite volume cells. *Computers and Fluids* 57, 225–236.
- Calhoun, D. A. (2002). Cartesian grid method for solving the two dimensional stream function vorticity equations in irregular regions. *Journal of Computational Physics* 176, 231– 275.
- Eisenlohr, H. and H. Eckelmann (1989). Vortex splitting and its consequences on the vortex street wake of cylinders at low Reynolds numbers. *Physics of Fluids* 1, 189–192.
- Gebhart, B., L. Pera and A. W. Schorr (1970). Steady laminar natural convection plumes above a horizontal line heat source. *International Journal of Heat Mass Transfer* 13, 161–171.
- Gerrard, J. H. (1978). The wakes of cylindrical bluff bodies at low Reynolds number. *Philosophical Transactions of the Royal Society Ser. A* 288, 351.
- Hama, F. R. (1957). Three-dimensional vortex pattern behind a circular cylinder. *Journal of Aeronautical Science* 24, 156–158.
- Karniadakis, G. E. and G. S. Triantafyllou (1992). Three-dimensional dynamics and transition to turbulence in the wake of bluff objects. *Journal of Fluid Mechanics* 238, 1– 30.
- Kieft, R. N., C. C. M. Rindt, A. A. van Steenhoven and G. J. F. van Heijst (2002, November). On the wake structure behind a heated horizontal cylinder in cross-flow. *Journal of Fluid Mechanics* 486, 189–211.
- Le, D. V., B. C. Khoo and J. Peraire (2006). An immersed interface method for viscous incompressible flows involving rigid and flexible boundaries. *Journal of computational physics* 220, 109–138.
- Lecordier, J. C., L. Hama and P. Paranthoen (1991). The control of vortex shedding behind heated circular cylinders at low Reynolds numbers. *Experiments in Fluids* 10, 224–229.
- Maas, W. J. P. M., C. C. M. Rindt and A. A. van Steenhoven (2003). The influence of heat on the 3D-transition on von Kármán vortex street. *International Journal of Heat and Mass Transfer* 46, 3069–3081.
- Mahir, N. (2017). Three dimensional heat transfer from a square cylinder at low reynolds numbers. *International Journal of Thermal Sciences* 119, 37–50.
- Mittal, S. and A. Raghuvanshi (2001). Control of vortex shedding behind circular cylinder for flows at low Reynolds numbers. *International Journal for Numerical Methods in Fluids* 35, 421–447.
- Rajani, B. N., A. Kandasamy and S. Majumdar (2016). LES of flow past circular cylinder at  $Re = 3900$ . *Journal of Applied Fluid Mechanics* 9(3), 1421–1435.
- Ren, M., C. C. M. Rindt and A. A. van Steenhoven (2004). Experimental and numerical investigation of the vortex formation process behind a heated cylinder. *Physics of Fluids*. 16(8), 3103–3114.
- Ren, M., C. C. M. Rindt and A. A. van Steenhoven (2006). Three-dimensional transition of water flow around a heated cylinder at  $Re=85$  and

- Ri=1. *Journal of Fluid Mechanics* 566, 195–224.
- Rolfo, S., K. Kopsidas, A. R. Shahnurriman, C. Moulinec and D. R. Emerson (2018). Effect of large scale 3D structures on the flow around a heated cylinder at low reynolds number. *Flow, Turbulence and Combustion* 101(2).
- Roshko, A. (1993). Perspectives of bluff body aerodynamics. *Journal of Wind Ind. Aerodyn* 49, 79–100.
- Russell, D. and Z. Jane Wang (2003). A cartesian grid method for modeling multiple moving objects in 2d incompressible viscous flow. *Journal of Computational Physics* 191, 177–205.
- Saad, Y. (2003). *Iterative Methods for Sparse Linear Systems 2nd Ed.* Philadelphia: Society for Industrial and Applied Mathematics.
- Sarkar, S., A. Dalal, and G. Biswas (2011). Unsteady wake dynamics and heat transfer in forced and mixed convection past a circular cylinder in cross flow for high Prandtl numbers. *International Journal of Heat and Mass Transfer* 54, 3536–3551.
- Sen, S., S. Mittal, and G. Biswas (2009). Steady separated flow past a circular cylinder at low Reynolds number. *Journal of Fluid Mechanics* 620, 89–119.
- Sparrow, E. M., R. B. Husar, and R. J. Goldstein (1990). Observations and other characteristics of thermals. *Journal of Fluid Mechanics*. 41, 793–800.
- Taneda, S. (1956). Experimental investigation of the wakes behind cylinders and plates at low Reynolds numbers. *Journal of the Physical Society of Japan*. 11, 302.
- Tanweer, S., A. Dewan, and S. Sanghi (2019). Study on effects of prandtl number on cross buoyancy flow past a square cylinder using openfoam. *Journal of Applied Fluid Mechanics* 12(1), 257–269.
- Vít, T., M. Ren, Z. Trávníček, F. Maršík and C. Rindt (2007). The influence of temperature gradient on the Strouhal-Reynolds number relationship for water and air. *Experimental Thermal and Fluid Science* 31, 751–760.
- Verzicco, R. and R. Camussi (1997). Transitional regimes of low-prandtl thermal convection in a cylindrical cell. *Physics of Fluids* 9, 1287–1295.
- Wang, A. B., Z. Travnicek and K. Chia (2000). On the relationship of effective reynolds number and strouhal number for the laminar vortex shedding of a heated circular cylinder. *Physics of Fluids* 12, 1401–1410.
- Williamson, C. H. K. (1988). The existence of two stages in the transition to threedimensionality of a cylinder wake. *Physics of Fluids* 31(11), 3165–3168.
- Williamson, C. H. K. (1996a). Mode-A secondary instability in wake transition. *Physics of Fluids* 8(6), 1680–1682.
- Williamson, C. H. K. (1996b). Three dimensional wake transition. *Journal of Fluid Mechanics* 328, 345–407.
- Williamson, C. H. K. (1996c). Vortex dynamics in the cylinder wake. *Annual Review of Fluid Mechanics* 28, 477–539.
- Williamson, C. H. K. and A. Roshko (1990). Measurements of base pressure in the wake of a cylinder at low Reynolds numbers. *Z. Flugwiss. Weltraumforsch.* 14, 38–46.
- Zdravkovich, M. M. (1997). *Flow around circular cylinders: Fundamentals*, Volume 1. Oxford University Press, New York.